Evaluation of Commercial CFD Code Capabilities for Prediction of Heavy Vehicle Drag Coefficients

W. David Pointer*
Argonne National Laboratory, Argonne, IL, 60439

In collaboration with the U.S. Department of Energy's Heavy Vehicle Aerodynamic Drag Team, Argonne National Laboratory is developing guidelines for the near-term use of existing commercial computational tools by the heavy vehicle manufacturing industry. These guidelines are being developed based upon measured drag coefficients as well as detailed surface pressure distributions from wind tunnel experiments completed at NASA Ames Laboratory using a generalized 1/8th-scale conventional U.S. tractor-trailer geometry, the Generic Conventional Model (GCM). Studies consider the effects of selection of global and near surface mesh size parameters and selection of turbulence modeling strategies. Initial results indicate that drag coefficients can be predicted within 1 percent of measured values and that reasonable agreement with measured surface pressure distributions can be achieved.

I. Introduction

The U.S. Department of Energy (DOE) supported Heavy Vehicle Aerodynamic Drag Team is a consortium of seven organizations pursuing the reduction of heavy vehicle fuel use through reduction in aerodynamic drag-related parasitic energy losses. Modern Class 8 tractor-trailers have wind average drag coefficients on the order of $C_D = 0.6$. At 70 miles per hour, as much of 65% of the total energy expended by a typical heavy truck vehicle can be consumed in overcoming aerodynamic drag. Since the energy losses resulting from aerodynamic drag increase as vehicle speed increases, vehicles traveling at higher speeds expend even more energy in overcoming aerodynamic drag forces. A reduction in the drag coefficient of such vehicles of 50% is not inconceivable and would result in a reduction in fuel use on the order of 25%[1]. Argonne National Laboratory is collaborating with other members of this consortium to develop guidelines for the application of existing commercial Computational Fluid Dynamics (CFD) software for the prediction of heavy vehicle aerodynamic drag. The goal of this project is to encourage and enable integration of computational modeling into the design processes of the heavy vehicle manufacturing community for near-term improvements in heavy vehicle aerodynamic design.

II. Selection of Commercial CFD Software

The guidelines developed by this program are intended to be generic advice for the application of a commercial CFD software package for the prediction of heavy vehicle aerodynamic drag coefficients. Since this market is currently dominated by finite volume formulations, the guidelines will focus upon software using this methodology. Preliminary guideline development will be completed using the commercial CFD code Star-CD.[2] The Star-CD software was selected for this purpose largely as a result of the flexibility in computational mesh development the code offers with the ability to utilize polyhedral "cut" cells and recognize both integral and arbitrary interfaces between regions of the computational domain. It is anticipated that the applicability of the general guidelines to other commercial CFD codes will be examined and that the extension of the guidelines to alternate commercial CFD software methodologies, such as Lattice-Boltzmann, will be pursued following the initial development stage.

III. The Generic Conventional Model

The Generic Conventional Model3 (GCM) is a generalized representation of a conventional U.S. tractor-trailer truck. The model is 1/8th scale, with approximate dimensions of 97 in. long by 13 in. wide by 21 in. high. The model is mounted at the center of the ground plane of a 10 ft. wide by 7 ft. high wind tunnel test section. Instrumentation includes a force balance, 476 steady pressure transducers, 14 dynamic pressure transducers, and

* Engineer, Nuclear Engineering Division, AIAA Member.

three-dimensional Particle Image Velocimetry (PIV). Data was collected at various Reynolds number values and yaw angles. Additionally, four different configurations of the GCM were considered in the experiments. The nominal configuration is a representative model of a current-generation tractor-trailer truck. Alternate configurations include the addition of a low-boy device under the length of the trailer, a full fairing between the cab and the trailer, and the combination of the fairing and low-boy device, as illustrated in Fig. 1. The initial studies presented herein consider only the case using the standard configuration of the GCM with a vehicle-width based Reynolds number of Re = 1.15 million and zero yaw angle. Measurements using alternate configurations, Reynolds numbers and yaw angles will be used to evaluate whether computational modeling guidelines developed based upon these studies are sufficiently general to be applied in the evaluation of the aerodynamic characteristics of other vehicles under different operating conditions.

IV. Computational Model

The computational model employed in these studies was developed using the ES-Aero tool for aerodynamic drag simulation that is available as part of the Star-CD software package. The surface of the standard configuration GCM is defined using approximately 500,000 triangular surface elements based upon CAD data representations taken from optical scans of the actual model. The computational domain is developed based upon this surface definition using a semi-automated process that begins by creating a hexahedral mesh that is successively refined in smaller zones around vehicle, with 4 cell to 1 cell coupling employed at the interfaces between zones. The dimensions of hexahedral elements that make up the innermost zone are specified by user as the near vehicle cell size. The mesh elements near the vehicle surface are then further refined based upon local surface features identified by the user or selected automatically based on curvature or gap width. The user specifies a minimum allowable cell size that limits the refinement of the mesh in this step.

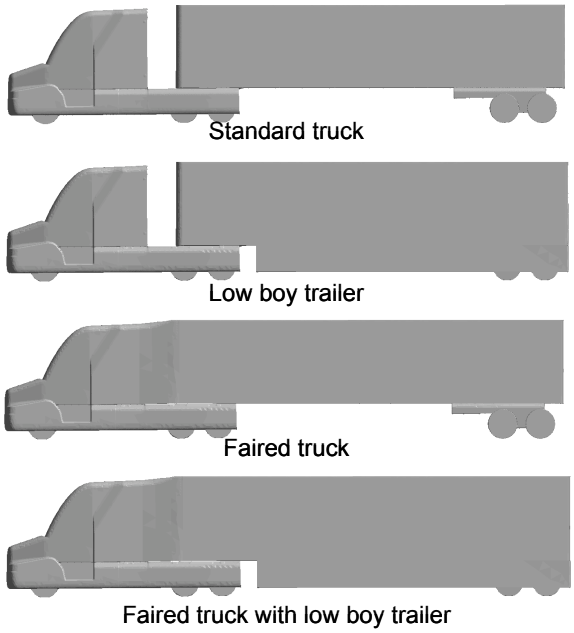

Figure 1. Generic Conventional Model (GCM) configurations.

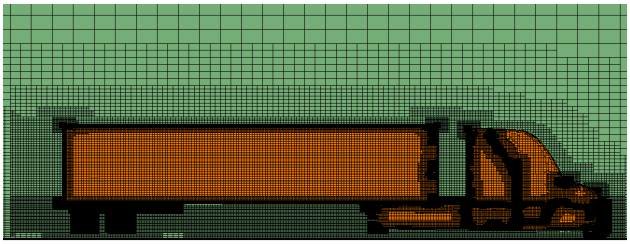

Figure 2. Example of computational mesh structure used in the simulation of the aerodynamic characteristics of Generic Conventional Model (GCM) configurations.

Using this locally refined hexahedral mesh, the original surface is "wrapped" by projecting the hexahedral mesh onto the original surface. In this manner, the multiple components defining the GCM are merged into a single surface. The "wrapped" surface definition is then volumetrically expanded to create a subsurface which is used to cut away the portions of the locally-refined hexahedral mesh that fall inside the vehicle. A brick and prism cell extrusion layer is then created to fill the gap between the sub-surface and the "wrapped" surface. In this way, the non-hexahedral cut cells are removed some distance from the surface. A final step further refines the wake region and the underbody region in order to better capture important flow features in those regions. An example of the mesh construction of the computational domain used in the GCM simulations is shown in Figure 2.

When using locally-refined, partially-unstructured computational domains with substantial numbers of non-hexahedral cells, the standard practice of evaluating grid convergence by uniformly refining the entire mesh in all directions becomes intractable. In the vehicle surface feature size based computational meshes used in these studies, two separate parameters determine the size of the mesh. The near vehicle cell size determines the bulk flow resolution surrounding the vehicle, and the minimum cell size determines the level of resolution allowed

as a result of feature-based refinement around significant features of the vehicles surface. Mesh sensitivity analyses included in these studies examine the effects of changes in these parameters upon the prediction of the drag coefficient, however, this is not equivalent to the traditional grid convergence study for two reasons. First, the grid is not uniformly refined in all directions throughout the domain. Second, the vehicle surface definition cannot be exactly maintained for all models since the final surface definition is dependent upon the local refinement of the computational mesh.

V. Bulk Flow Resolution

Five unique computational domains were generated based upon the standard GCM configuration in order to evaluate the effects of the near vehicle cell size parameter on the prediction of the drag coefficient. Near-vehicle cell sizes of 16.0, 12.0, 10.0, 8.0 and 6.0 mm were considered. In each case, the minimum cell size resulting from local feature-based refinements is 12.5 percent of the near vehicle cell size and an additional restriction is set so that a minimum of 16 elements are required for the definition of a circle. In order to ensure that the quality of the vehicle surface is maintained, the cell layer immediately adjacent to the surface is refined to 25 percent of the original size prior to trimming. The computational domain characteristics are shown in Table 1.

Table 1. Summary of computational domain characteristics for evaluation of bulk cell size effects.

Near Vehicle Cell Size (mm)	Minimum Cell Size (mm)	Total Number of Volume Elements	Number of Volume Elements on Surface
16.0	2.0	1012338	73574
12.0	1.5	1737085	126119
10.0	1.25	2345640	175105
8.0	1.0	3282426	266666
6.0	0.75	5695622	400382

Table 2. Summary of computational cost for each case considered in the evaluation of bulk cell size effects.

Near-Vehicle Cell Size (mm)	Total CPU Time (seconds)	Total Clock Time (seconds)
16	206072	16454
12	390113	29392
10	417686	32182
8	610958	44967
6	2720956	188577

Table 3. Effects of Near-Vehicle Cell Size Parameter on Accuracy of Drag Coefficient Prediction.

Near-Vehicle Cell Size (mm)	Predicted Drag Coefficient	Error in Drag Coefficient
experiment	0.398	
16	0.449	12.0
12	0.441	10.3
10	0.418	4.9
8	0.415	4.2
6	0.405	1.7

Each computational domain was considered in a parametric study for evaluation of the sensitivity of the prediction of the vehicle drag coefficient to changes in the bulk flow resolution. A uniform velocity of 51.45 m/s, corresponding to a Reynolds number of 1.1×10^6 was specified at the inlet, and a zero gradient condition is specified at the outlet. In these simulations, the standard high Reynolds number two-equation k-_ turbulence model and a logarithmic wall function are employed for prediction of turbulent kinetic energy and dissipation.

For each case, 3000 iterations were calculated using Star-CD's standard conjugate gradient solver and the PISO predictor-corrector algorithm. Convergence criteria were set to insure that all cases would reach 3000 iterations before stopping. At the 3000th iteration, all residuals are less than 10^{-4}. In addition to standard flow variable residual monitoring for the mass, momentum and energy equations, the drag coefficient of the vehicle is monitored as the solution develops to insure that the drag coefficient reaches a converged. Total computational time and clock time when using 16 processors for each simulation are shown in Table 2.

Predicted drag coefficients from each of the five cases are compared with experimental data from wind tunnel tests in Table 3. While there is a trend of improvement with reduction in near-vehicle cell size, the effects that lead to non-linearity in the trend are not immediately clear. More detailed comparisons of pressure distributions on the surface of the vehicle provide better insight into the sensitivity of the predictive capability to the bulk flow resolution. The pressure coefficient distribution on the surface of the vehicle from the case using the mesh based upon an 8mm near vehicle cell size is shown in Figure 3 as an example of a typical predicted pressure distribution on the vehicle surface. Pressure coefficient data was extracted along the centerline of the vehicle for each case and compared with experimental data as shown in Figure 4. These comparisons show that the difference in the accuracy

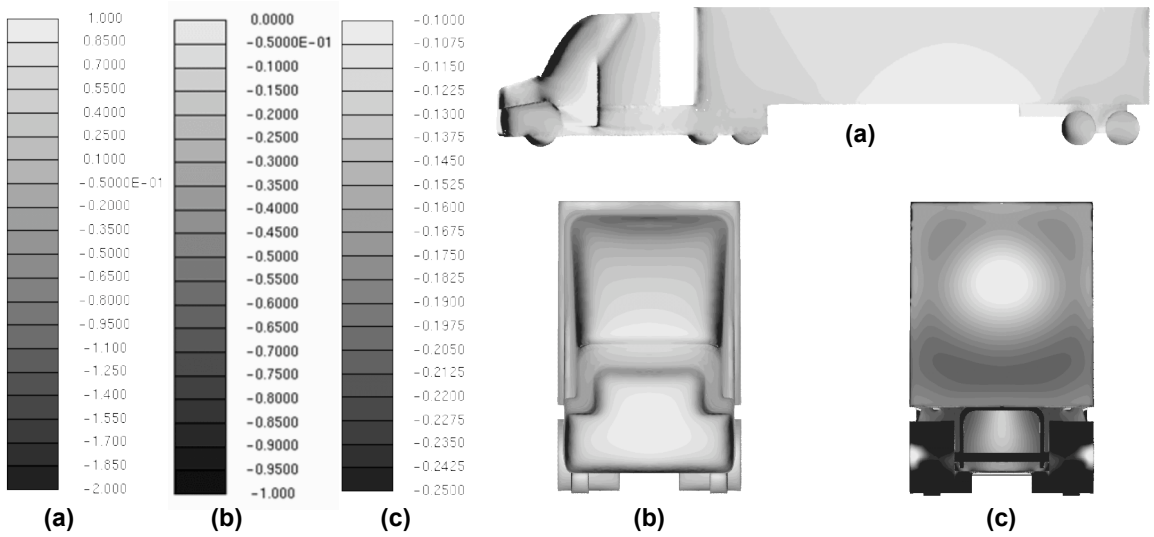

Figure 3. Predicted pressure coefficient distribution on the vehicle surface. Shown are (a) the side view of the full vehicle, (b) the front of the tractor, and (c) the base of the trailer.

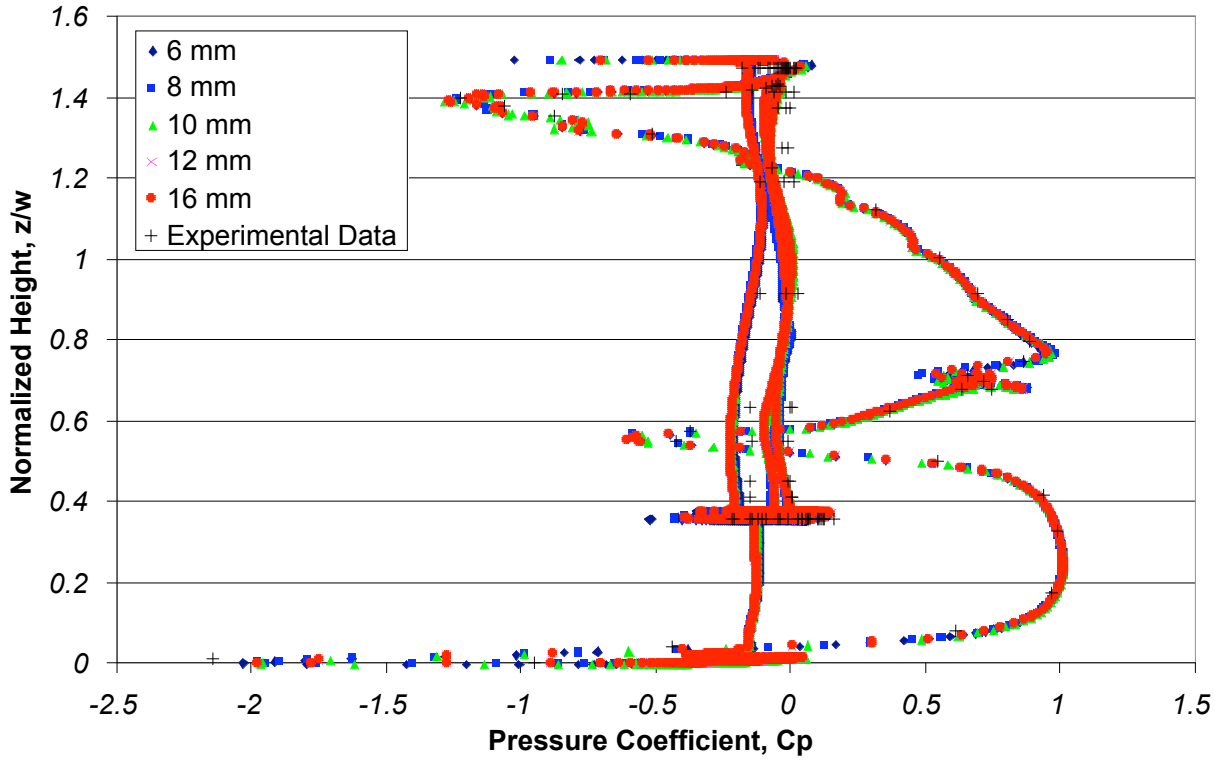

Figure 4. Comparison of predicted pressure coefficient distributions on the vehicle surface for various values of the near vehicle cell size parameter with experimental data for the GCM geometry.

of the drag coefficient prediction as a function of the near vehicle cell size is a result of small differences in the pressure distribution over the entire surface rather than large localized differences.

VI. Near Wall Resolution

Following the assessment of the effects of the near-vehicle cell size parameter on the accuracy of the drag coefficient prediction, the effect of the near-wall cell size parameter was also considered. The near-vehicle cell size was set to 8mm and the minimum cell size for local refinement was reduced from 1mm to 0.5 mm. The change in the near wall resolution increases the number of computational elements from 3,282,426 to 4,264,232. When selecting near wall cell size limits, it is important to consider the appropriate limits of the parameter y^+, which describes the thickness of the region near the wall where the logarithmic law of the wall function is applied. For the turbulence model and wall function employed in these studies, the value of y^+ should fall between 20 and 200. A near-wall computational cell that is too small will result in a value of y^+ that is too small, and a near-wall computational cell that is too large will result in a y^+ that is too large. As shown in Figure 5, the value of y+ falls within the appropriate range for the turbulence model employed.

A simulation of the flow of air over the vehicle was completed using the refined computational mesh for comparison with the previous simulations. As in the previous cases, a uniform inlet velocity condition and a zero gradient outlet condition were specified, and the standard high Reynolds number k-_ model was utilized. Convergence criteria were set so that 3000 iterations were completed, and all residuals fall below 10^{-4} by the 3000^{th} iteration. The change in the computational mesh resolution results in a increase in the total CPU time from 610,958 seconds to 703,027 seconds.

The change in the near-wall refinement parameter results in a reduction in the error of the drag coefficient prediction from 4.2 percent to 1.0 percent. The predicted surface pressure distributions along the vehicle centerline for both cases are shown in Figure 6 along with the experimentally measured pressure distribution. As in the assessment of the effects of the near vehicle cell size parameter, comparisons of surface pressure data indicate that differences in drag coefficient predictions are a result of small differences in the predicted surface pressure distributions over the entire vehicle rather than large localized discrepancies.

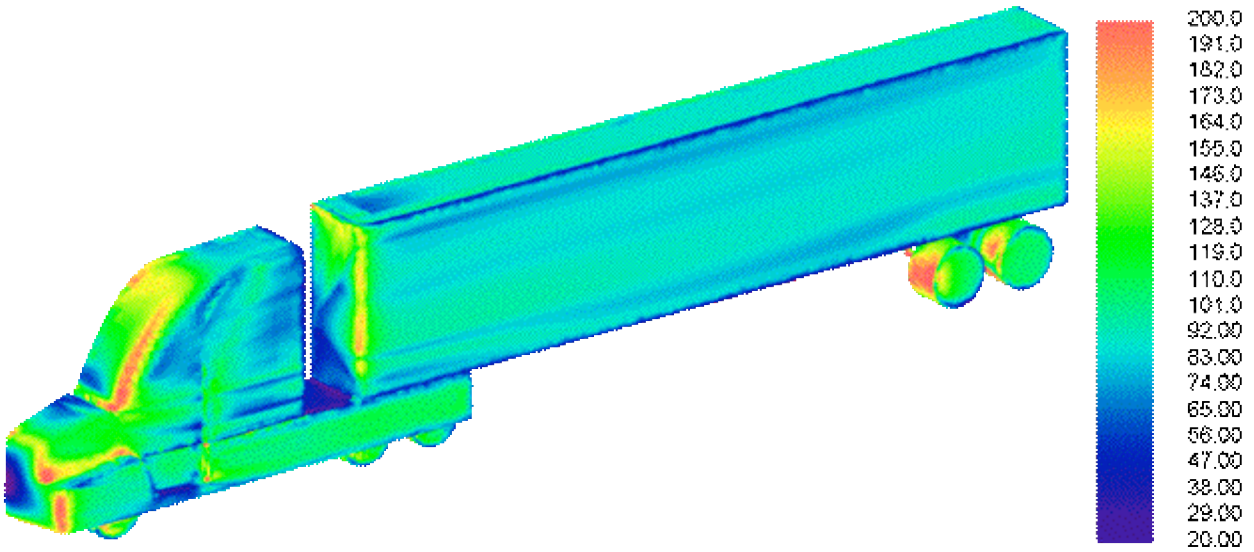

Figure 5. Values of the y^+ parameter along the surface of the computational model of the GCM geometry when the computational mesh uses a near-vehicle cell size of 8 mm and a near-wall cell size limit of 1 mm.

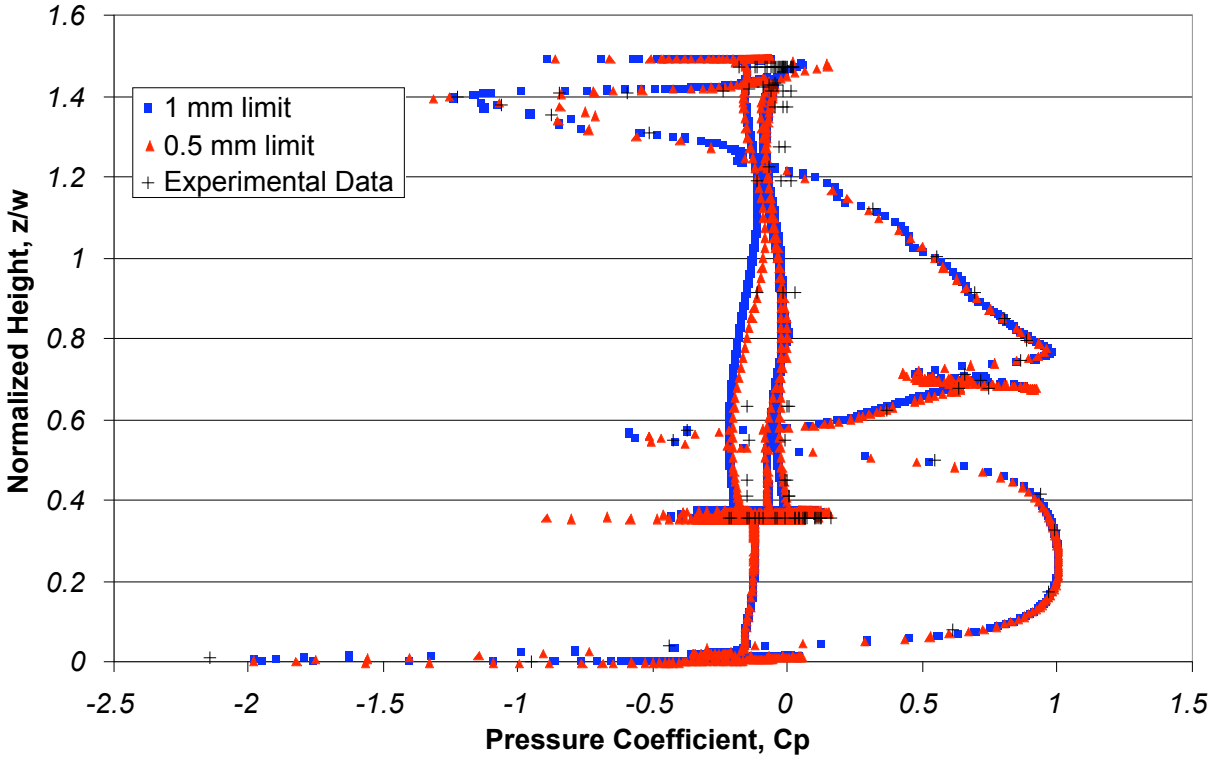

Figure 6. Comparison of predicted pressure coefficient distributions on the vehicle surface for various near wall cell size limits with experimental data for the GCM geometry.

VII. Turbulence Model Selection

In all simulations completed as part of the computational mesh sensitivity studies, the high Reynolds number k-_ turbulence model was used in conjunction with a standard logarithmic wall function for the prediction of turbulent kinetic energy and eddy diffusivity. While the high Reynolds number k- _ turbulence model is a robust general purpose turbulence model, the strong adverse pressure gradients and large flow recirculation regions associated with the GCM geometry may limit the applicability of steady state Reynolds Averaged Navier-Stokes (RANS) modeling strategies. Therefore, the sensitivity of the drag coefficient prediction to the choice of two equation steady RANS turbulence model was also assessed.

Using the computational mesh with a near vehicle cell size of 8 mm and a near wall cell size limit of 1 mm, simulations of the aerodynamic characteristics of the GCM model were repeated using five steady RANS turbulence models and their associated wall functions:

1) the standard high-Reynolds number k-_ model with logarithmic wall function
2) the Menter k-_ SST model
3) the renormalization group (RNG) formulation of the k-_ model
4) the Chen formulation of the k-_ model
5) the quadratic formulation of the k-_ model

The standard k-_ model and the k-_ SST model are identical in the far field, but the k-_ SST model incorporates additional detail in the near wall region and in separated flow regions. The RNG model is similar to the standard k-_ model, but includes an additional term to account for the mean flow distortion of the dissipation. Chen's model is also similar to the standard k-_ model, but includes an additional term to more effectively account for the effects of changes in the mean strain rate on the energy transfer mechanism of turbulence. The quadratic model is a higher order model of the k-_ type that includes non-linear terms to allow for the anisotropy of turbulence in some flow fields.

As in the previous cases, a uniform inlet velocity condition and a zero gradient outlet condition were specified, and the standard high Reynolds number k-_ model was utilized. Convergence criteria were set so that 3000 iterations were completed, and all residuals fall below 10^{-4} by the 3000^{th} iteration. The drag coefficients predicted using each of the selected steady-RANS turbulence models are shown in Table 4. More detailed comparisons of the predicted pressure coefficient distributions when using each of the selected turbulence models are shown in Figure 7. Unlike previous studies, the differences in the predicted drag coefficient are largely a result of localized discrepancies in the surface pressure coefficient predictions in the regions of separated flow, as shown in Figure 8.

Table 4. Results of the evaluation of two-equation turbulence models for prediction of drag coefficients for the GCM geometry.

Turbulence Model	Predicted Drag Coefficient	Percent Error in Prediction
Experiment	0.398	--
High-Reynolds Number k-epsilon Model	0.402	1.0
Menter k-_ SST model	0.401	0.8
RNG model	0.389	2.3
Chen's model	0.3919	1.61
Quadratic model	0.3815	4.32

The differences in the predictions of the surface pressure distribution are a direct result of differences in the predicted flow fields. The predicted velocity magnitude at the centerline is shown for each selected turbulence model in Figure 9. The primary differences in velocity field prediction occur in the recirculation zone under the trailer and in the interaction between the underbody flow and the separated flow region at the trailer base. The location of these differences correspond to the largest discrepancies between the surface pressure distribution predictions.

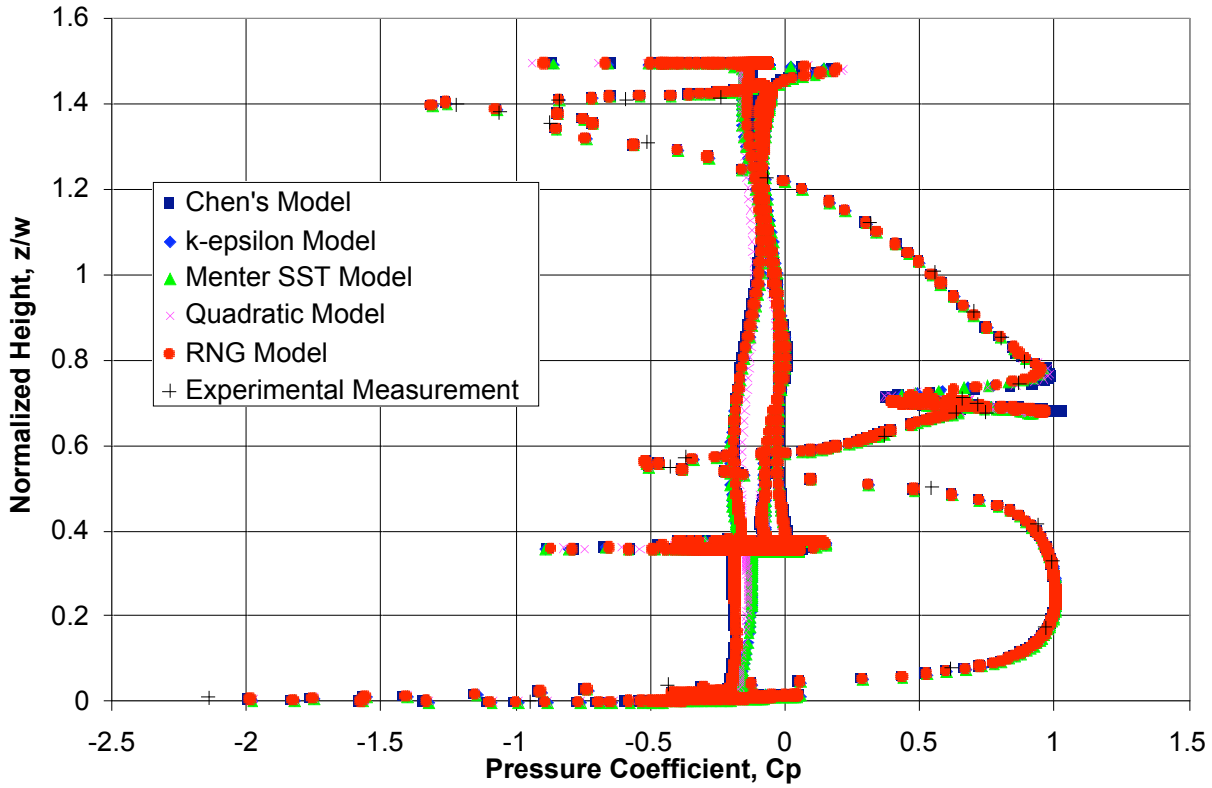

Figure 7. Comparison of predicted pressure coefficient distributions on the vehicle surface with experimental data for selected turbulence models.

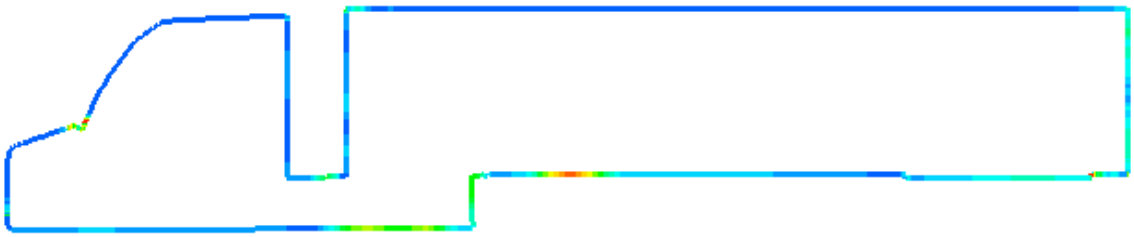

Figure 8. Standard deviation of the surface pressure distribution predictions using the selected turbulence models.

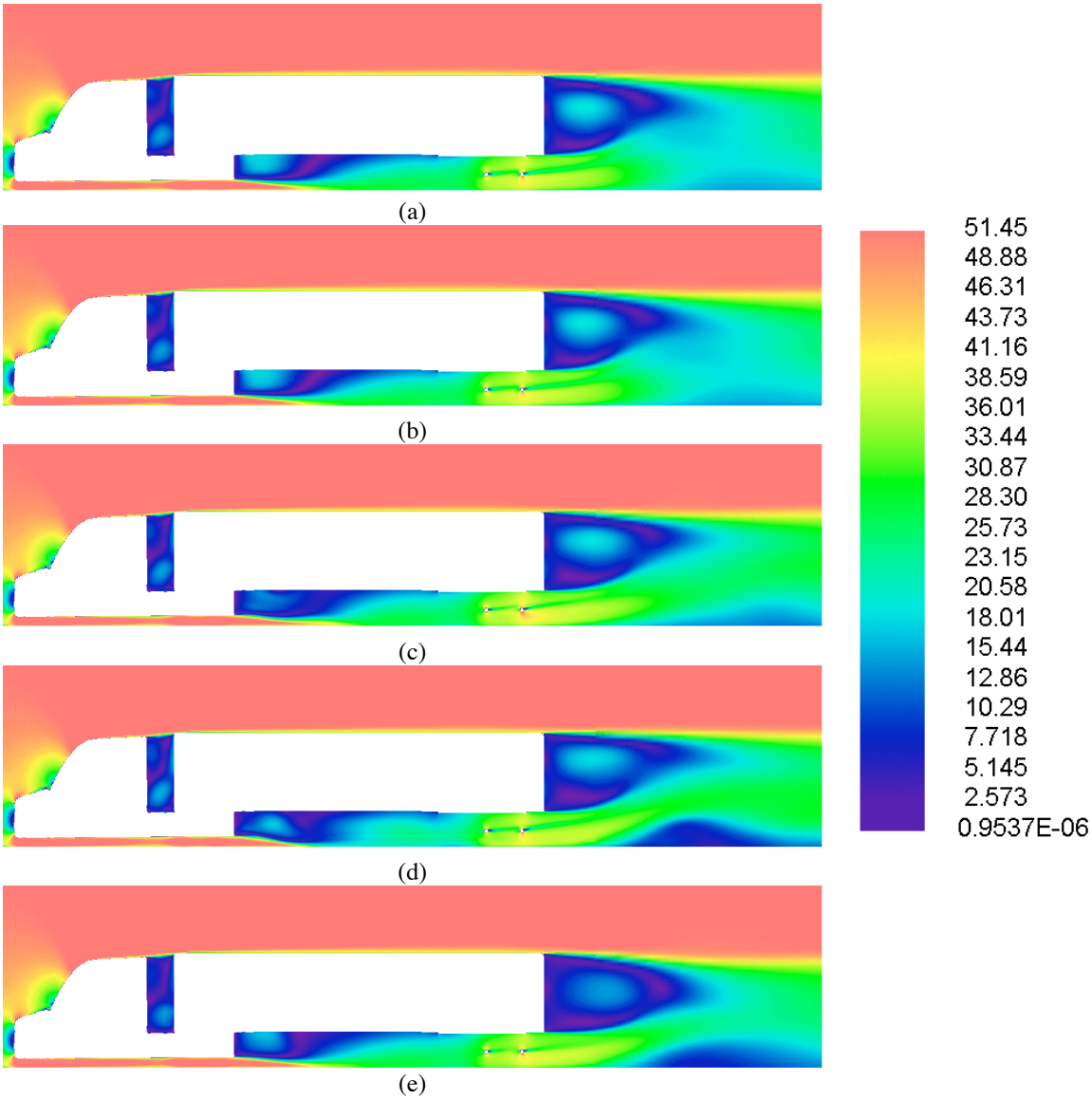

Figure 9. Comparison of predicted steady state velocity fields for five selections of turbulence model: (a) the standard high-Reynolds number k-_ model with logarithmic wall function, (b) the Menter k-_ SST model, (c) the renormalization group (RNG) formulation of the k-_ model, (d) the Chen formulation of the k-_ model, and (e) the quadratic formulation of the k-_ model.

VIII. Full Vehicle versus Half Vehicle

In order to evaluate the effects of considering only half of the vehicle rather than the full vehicle, two models were created using the full vehicle geometry. These models use the same mesh parameter settings as the two coarsest models considered in the mesh sensitivity study. The full vehicle models are based upon near-vehicle cell sizes of 12 mm and 16 mm, with minimum near-wall cell sizes of 1.5 mm and 2.0 mm respectively. As in all previous studies, 3000 iterations were completed for each steady-state simulation and the convergence of the drag coefficient was monitored.

As shown in Table 5, drag coefficient predictions show a slight improvement in agreement with experimental measurements when the full-vehicle model is used. The comparison of more detailed pressure coefficient distributions along the vehicle surface, as shown in Figure 10, reveal that the most substantial discrepancies between the full and half vehicle model predictions occur along the underbody and in the gap between the tractor and trailer. The GCM geometry is in reality slightly asymmetric and the consideration of this geometric asymmetry is likely the primary difference in the models that contributes to these discrepancies.

Table 5. Comparison of drag coefficient predictions from half-vehicle and full-vehicle models.

	Half-Vehicle	
Near-Vehicle Cell Size (mm)	**Predicted Drag Coefficient**	**Percent Error in Prediction**
16	0.449	12.0
12	0.441	10.3
	Full- Vehicle	
	Predicted Drag Coefficient	**Percent Error in Prediction**
16	0.441	10.3
12	0.426	6.7

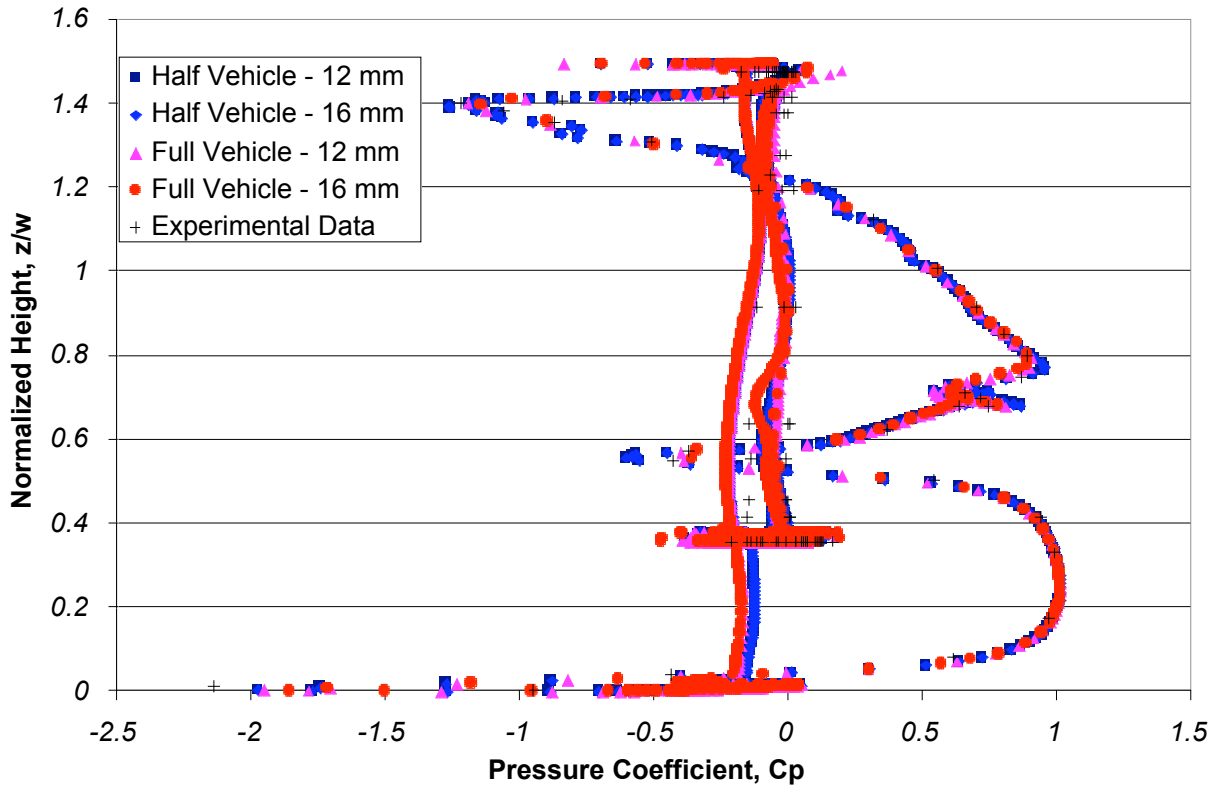

Figure 10. Comparison of predicted pressure coefficient distributions on the vehicle surface when the full vehicle model is used with predicted pressure coefficient distributions when the half vehicle model is used and with experimental data.

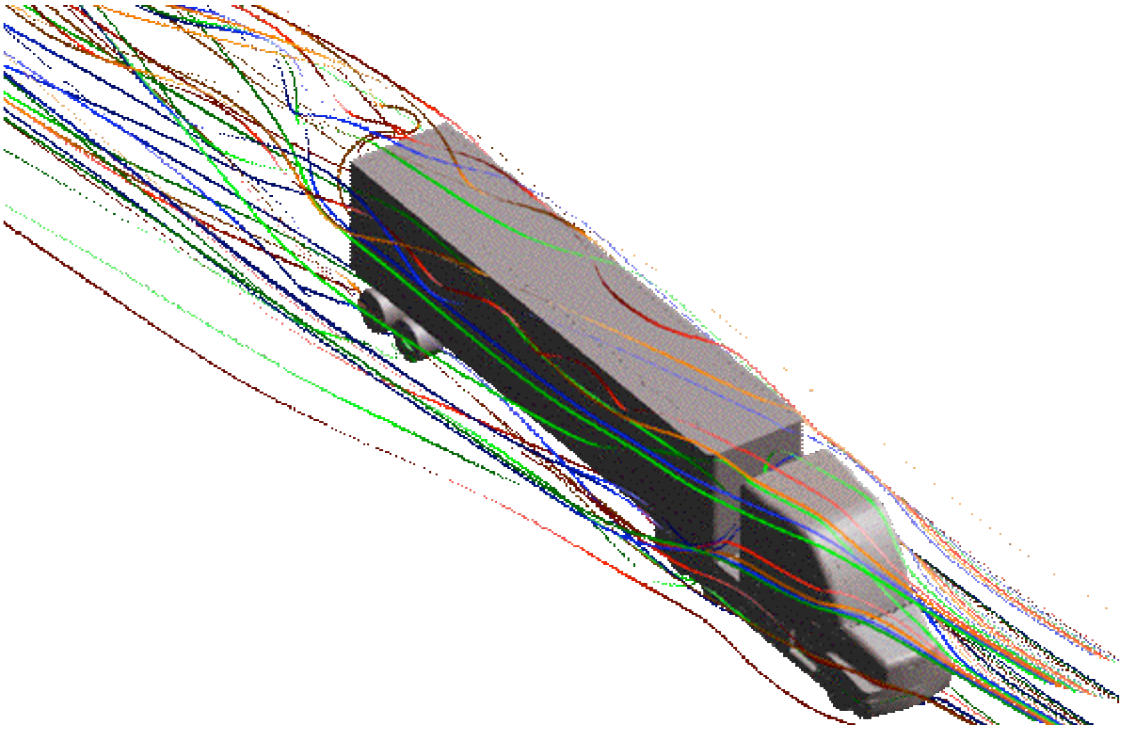

Figure 11. Predicted streamlines across the surface of the GCM geometry when the vehicle is placed at a yaw angle of 10 degrees.

IX. Future Work

Ongoing efforts will focus upon the assessment of the capabilities within current generation software using simple steady RANS modeling strategies for the prediction of changes in drag with changes in geometry or flow conditions. These efforts will consider the standard configuration of the GCM geometry at yaw angles greater than zero degrees, as shown in Figure 11, as well as the alternate configurations of the GCM geometry shown in Figure 1. Upon completion of computational studies for each configuration of the geometry, predictions of drag coefficient and surface pressure distributions will be compared with experimentally measured values for that configuration.

X. Conclusions

These studies are the initial component of an assessment of the capabilities for the prediction of heavy vehicle aerodynamic characteristics using current generation commercial computational fluid dynamics software. Based upon the outcomes of these studies, guidelines are being developed for the immediate application of these current generation tools by the heavy vehicle manufacturing community. Initial assessments have shown that drag coefficients can be predicted within less than 1 percent of the measured value and the surface pressure distributions can be predicted with reasonable accuracy.

Acknowledgments

This work has been completed under the auspices of the U.S. Department of Energy by the University of Chicago as Operator of Argonne National Laboratory ("Argonne") under Contract No. W-31-109-ENG-38.

References

[1] McCallen, R., et al., "DOE's Effort to Reduce Truck Aerodynamic Drag – Joint Experiments and Computations Lead to Smart Design," AIAA Fluid Dynamics Conference, AIAA, Washington, DC, 2004. (in publication)

[2] Star-CD, version 3.150A, CD-Adapco Group, Melville, NY.

[3] Satran, D., "An Experimental Study of the Generic Conventional Model (GCM) in the NASA Ames 7-by-10-Foot Wind Tunnel," United Engineering Foundation Conference on The Aerodynamics of Heavy Vehicles: Trucks, Buses, and Trains, United Engineering Foundation, New York, 2002. (in publication)